doi.org/10.1002/batt.202000261

Special Collection

Unravelling the Role of Speciation in Glyme:Ionic Liquid Hybrid Electrolytes for Na–O_2 Batteries

Laura Garcia-Quintana,[a] Fangfang Chen,[a] Nagore Ortiz-Vitoriano,*[b, c] Yafei Zhang,[a] Luke A. O'Dell,[d] Douglas R. MacFarlane,[e] Maria Forsyth,[a, c] Alan M. Bond,[e] Patrick C. Howlett,[a] and Cristina Pozo-Gonzalo*[a]

The morphology and size of the discharge products in Na–O_2 batteries are largely dominated by the interactions of the electrolyte with superoxide and sodium ions; therefore, an in-depth understanding is essential for achieving high performance batteries. Herein, we report a framework designed to understand solvation and coordination in the recently discovered hybrid electrolytes, based on glyme and a pyrrolidinium ionic liquid. FTIR and NMR spectroscopic techniques, coupled with molecular dynamics simulations, have been used to characterize these systems. We demonstrate that the presence of ionic liquid in the hybrid electrolyte affects the superoxide coordination environment by weakening the glyme-Na^+ interactions, and generating solvent separated ion pairs. All these factors lead to different deposition mechanisms, which will determine the battery performance. The Na^+ solvation shell compositions, anion conformers and relative free glyme content are also evaluated. The combinatorial approach used in this study-experimental and computational – can be applied for further design of these hybrid electrolytes and other metal – O_2 chemistries and electrochemical systems.

1. Introduction

Current energy demands require the development of energy storage technologies with higher energy density, but that can also be produced in a more sustainable manner. Among the next generation energy storage technologies, metal-O_2 batteries have attracted a great deal of attention. Na–O_2 batteries have been of particular interest because of their high energy density (1605 or 1108 $W\,h\,kg^{-1}$, depending on the discharge products), use of abundant raw materials and a high energy density metallic Na anode, which reduces the overall production costs.[1]

It is well known that two different discharge products can be obtained in a Na–O_2 battery during the discharge process: the superoxide NaO_2 ($E^0 = 2.27$ V vs $Na^{+/0}$) which is kinetically favoured, and/or the peroxide Na_2O_2 species ($E^0 = 2.33$ V vs $Na^{+/0}$) which is thermodynamically favoured.[1a,2] Recent studies have shown that the choice of electrolyte influences the chemistry and morphology of the discharge products, which are in turn governed by the deposition mechanism and solvation effect of the ion pairs.[3]

Organic solvents, especially glyme-ether based solvents, have been widely used in Na–O_2 batteries due to their compatibility with Na metal and their stability against superoxide.[2b,4] Lutz et al. reported a dependence between the alkyl chain length of the glyme and battery performance.[4a] The authors associated the alkyl chain/battery capacity correlation to both the solubility of the discharge products and the particle size of the NaO_2 deposits generated during discharge. Thus, the generation of small particles led to passivation of the air cathode and consequential failure of the battery. On the other hand, bigger deposits led to the generation of a 3D structured layer that enabled O_2 to flow through the battery, delaying battery failure. Ortiz-Vitoriano et al. further supported these findings and demonstrated that the size and dynamics of the glyme affects the charge/discharge rate in Na–O_2 batteries, and therefore the overall cell performance.[3] The effect of sodium salt concentration on the morphology of the discharge products has been studied by Tatara et al.[5] They demonstrated a concentration dependence of the discharge capacity and morphology, where both parameters increased with the sodium concentration up to a maximum and then decreased.

[a] L. Garcia-Quintana, Dr. F. Chen, Dr. Y. Zhang, Prof. M. Forsyth, Prof. P. C. Howlett, Dr. C. Pozo-Gonzalo
ARC Centre of Excellence for Electromaterials Science
Institute for Frontier Materials
Deakin University
Geelong, Victoria 3200, Australia
E-mail: cristina.pozo@deakin.edu.au
[b] Dr. N. Ortiz-Vitoriano
Centre for Cooperative Research on Alternative Energies (CIC energiGUNE)
Basque Research and Technology Alliance (BRTA)
Parque Tecnológico de Alava
Albert Einstein 48, 01510 Vitoria-Gasteiz, Spain
E-mail: nortiz@cicenergigune.com
[c] Dr. N. Ortiz-Vitoriano, Prof. M. Forsyth
Ikerbasque, Basque Foundation for Science
María Díaz de Haro 3, 48013 Bilbao, Spain
[d] Dr. L. A. O'Dell
Institute for Frontier Materials
Deakin University
Geelong, Victoria 3216, Australia
[e] Prof. D. R. MacFarlane, Prof. A. M. Bond
ARC Centre of Excellence for Electromaterials Science
Monash University
Clayton, Victoria 3800, Australia

Supporting information for this article is available on the WWW under https://doi.org/10.1002/batt.202000261

Special Collection An invited contribution to a joint Special Collection between ChemElectroChem and Batteries & Supercaps dedicated to research Beyond Lithium-Ion Batteries

The authors suggested that this effect was due to two competing mechanisms occurring in the electrolyte: the effect of the free dimethoxyethane (DME) versus the effect of the Na^+ on the solubility and, in turn, the stabilization of NaO_2.

Although many studies have used these glyme-based electrolytes, their stability is insufficient due to the strong nucleophilic attack of the electrogenerated superoxide generated during discharge.[6] This leads to the formation of reaction intermediates such as singlet oxygen which is highly reactive and drives the formation of carbonates, oxalates and formates among others, which cause cell failure.[7]

Ionic liquids (ILs) have arisen as a new generation of electrolytes due to their low vapour pressure, high electrochemical and chemical stability, and efficient and stable Na metal plating and stripping.[8] *N*-butyl-*N*-methylpyrrolidinium bis(trifluoromethane-sulphonyl)imide ([C_4mpyr][TFSI]) is one of the most studied electrolytes in metal-O_2 batteries due to its high oxygen redox reversibility and stability in Na^+/Na electrochemistry.[9] Recently, we have studied the effect of salt concentration in the [C_4mpyr][TFSI] IL, where an increase in discharge/charge capacities, as well as particle size and distribution, was observed upon increasing the sodium bis (trifluoromethanesulphonyl)imide (NaTFSI) concentration.[10] However, the highest concentration of salt used in this prior study was limited to only 16.6 mol% (*ca.* 0.5 m), which is close to the saturation point.

It has recently been reported that superconcentrated electrolytes (those where the salt concentration approaches 50 mol%) improve target ion mobility and in turn, the device performance.[11] On the other hand, the use of hybrid electrolytes have emerged as a valid strategy to increase the salt concentration in the electrolyte. Thus, the combination of diethylene glycol dimethyl ether (DGME) and [C_4mpyr][TFSI] significantly increases the maximum possible NaTFSI salt concentration, up to 35 mol% NaTFSI. These hybrid solvents combine the best properties of both components: ILs act as fire retardants, compared to the traditional flammable organic solvents used, hence increasing safety. It is well known from the literature that the addition of ionic liquids to organic solvents (e.g. pyrrolidinium-carbonate solvents) can control the flammability and volatility, and even lead to non-flammable hybrid electrolytes.[12] Glymes, by contrast reduce the viscosity of the ILs, therefore increasing Na^+ mobility.

Our recent research reported the electrochemical performance of Na–O_2 batteries using two different salt concentrations (16.6 (0.5 m) and 35 mol% (2.8 m) NaTFSI) in the ([C_4mpyr][TFSI]:DGME) hybrid electrolyte, which in both cases showed longer cyclability despite the lower capacity when compared with the pure glyme system (Figure 1).[13] The less concentrated electrolyte mixture led to larger and more homogenous discharge products. Additionally, fewer side products were observed in the less concentrated electrolyte, which is essential for battery reversibility. We hypothesised that the strength of electrolyte-discharge products interactions dictated the deposition mechanism.

In this work, we correlate the Na^+-electrolyte interactions in the 16.6 and 35 mol% NaTFSI /[C_4mpyr][TFSI]:DGME hybrid

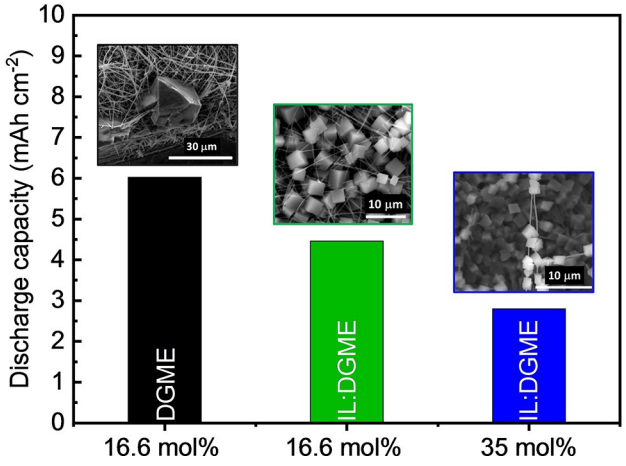

Figure 1. Column graph representing the discharge capacity for the two compositions used in this work (16.6 and 35 mol%/IL:DGME) and the glyme-based electrolytes along with the corresponding air cathode micrographs. Adapted figure from Ref. [13] with permission. Copyright (2020), American Chemical Society.

electrolytes to the deposition mechanism and implications for battery performance. Thus, both experimental (FTIR, NMR) and computational approaches are exploited, also considering the presence of superoxide anion which is normally overlooked in the literature. The research presented here provides further information on the reason behind the growth mechanism of the discharge products, building on the battery performance obtained from our previously reported work,[13] and developing the basis of electrolyte design needed to underpin future research in the field.

2. Results and Discussion

2.1. FTIR Spectroscopy

To study the interactions between Na^+ and the electrolyte – the chemical structures of the different species present in the hybrid electrolyte are shown in Figure 2 –, Fourier transform infrared (FTIR) spectroscopy was performed, focusing on the main bands of the TFSI anion and DGME as the solvating species.

Results were compared with those obtained for both neat [C_4mpyr][TFSI] and DGME (in the absence of Na^+). For clarification, there is an excess of DGME (four molecules of DGME per Na^+) in the 16.6 mol%/IL:DGME; whereas the 35 mol%/IL:DGME presents a deficiency of DGME to fully coordinate Na^+ (1.5 molecules of DGME per Na^+). In addition, different electrolyte mixtures with the same concentrations (16.6 and 35 mol% NaTFSI) were prepared in the presence of only one of the solvents (DGME or [C_4mpyr][TFSI]) to provide the relevant control experiments (Table 1).

The spectrum for the neat DGME contains two main bands that correspond to the stretching of OCCO bonds. One band is due to OCCO antisymmetric stretching at 1102 cm^{-1} and the

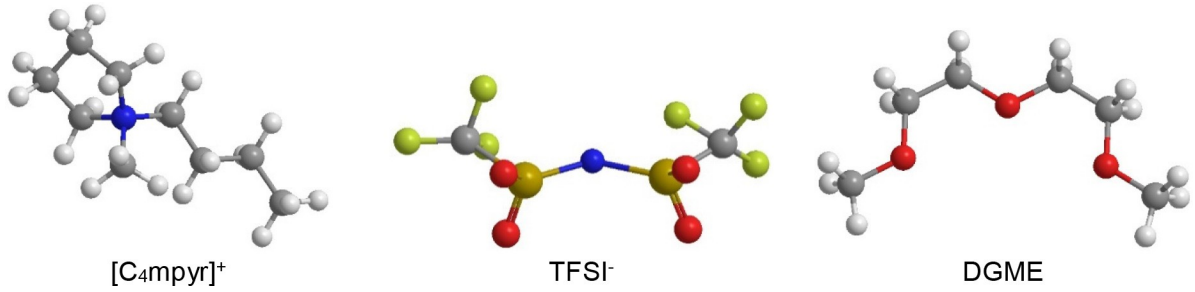

Figure 2. Chemical structures of the different species present in the hybrid electrolyte: $[C_4mpyr]^+$, $TFSI^-$ and DGME.

Table 1. Composition of the samples studied as the mole ratio of each component versus one mole of Na^+. Note mol% refers to the concentration of NaTFSI in the electrolyte.

Sample	Mole ratio			
	C_4mpyr^+	DGME	$TFSI^-$	Na^+
16.6 mol%/IL	5	0	6	1
35 mol%/IL:DGME	0.4	1.5	1.4	1
35 mol%/DGME	0	1.9	1	1
16.6 mol%/IL:DGME	1	4	2	1
16.6 mol%/DGME	0	5	1	1

second at 853 cm^{-1} is a mixture of OCCO symmetric stretching and CH_2 rocking vibrations (Figure 3a and b, respectively).[14]

Both bands split into two bands in the presence of Na^+, which are located at higher and lower wavenumbers. Similar behaviour was reported by Tatara et al., in a NaTFSI/DME mixture, where three bands were identified by Raman spectroscopy: one for coordinated DME at 865 cm^{-1} and two corresponding to free DME in the range of 800–860 cm^{-1}.[5] The authors also reported an increase in the intensity of the coordinated DME and a decrease of free DME bands upon increased Na^+ salt concentration. Moreover, Geyens et al. reported a similar trend in an electrolyte composed of varying concentrations of sodium bis(fluorosulfonyl)imide in DGME.[4b]

The nature of the two different bands for coordinated DGME is correlated with a change in the backbone structure of the DGME due to changes in the torsional angles of the OCCO structure, which has previously been observed in glymes in the presence of Na^+ and Li^+.[4b,14a,15] To further understand the contributions of these bands, the FTIR spectra were fitted in the 900–800 cm^{-1} region (Figure 4). Fitting of the neat DGME was conducted using a simplified version of this multiband, showing only three of the contributions which are identified as *trans* (824 and 879 cm^{-1}) and *gauche* (853 cm^{-1}) conformers, based on previous studies.[14b,16] Further fitting of the different electrolyte compositions showed five components in this region related to free and coordinated glyme. The contribution of coordinated DGME in the concentrated electrolytes (35 mol% NaTFSI in either DGME or IL:DGME) is above 90% (94 and 97%, respectively), independent of the solvent. However, a small contribution of free DGME (<7%) is present due to the dynamic equilibrium of these species in the electrolyte. In contrast, the contribution of free DGME in the less concentrated electrolytes is larger and strongly depends on the electrolyte composition (29% and 64% for the 16.6 mol% NaTFSI in IL:DGME and DGME, respectively). The variation in free DGME between the 35 mol% and 16.6 mol% IL:DGME is expected due to the excess of DGME in the less concentrated electrolytes. The free DGME will affect the physicochemical properties of the electrolyte, and hence, the mass transport. This is shown in Table 3 and the implications will be discussed later in the manuscript.

Another ligand present in these electrolyte mixtures is the TFSI anion, whose coordination in the presence of sodium salt is important to understand. The TFSI anion presents different

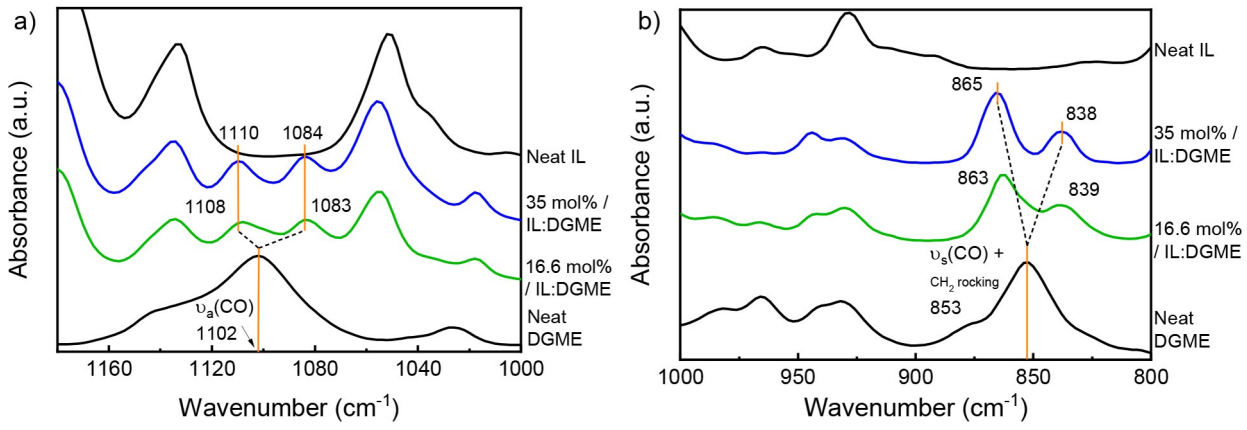

Figure 3. FTIR spectra of the neat DGME and IL along with the 16.6 and 35 mol%/IL:DGME mixtures in the region of a) 1170–1000 cm^{-1} and b) 1000–800 cm^{-1}.

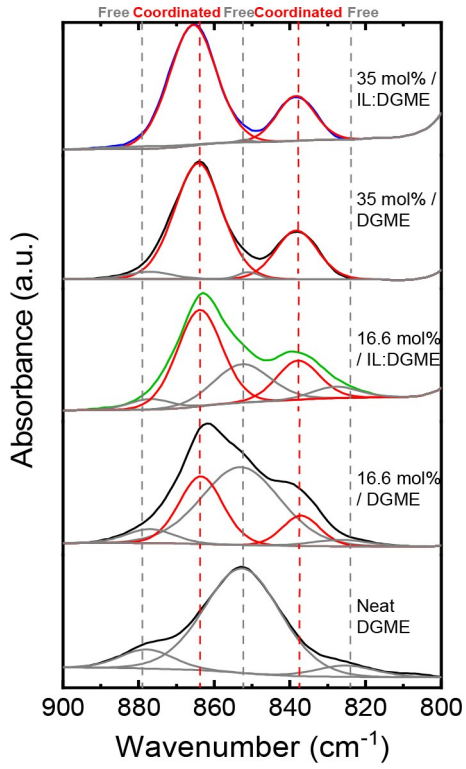

Figure 4. Fitting of the FTIR spectra in the 900–800 cm^{-1} region for all the compositions, showing the variation of free DGME (grey curve) vs coordinated DGME (red curve) upon DGME concentration.

Table 2. Relative intensities of the *cis/trans* conformers contributing to the SO_2 antisymmetric stretching band at 1340 cm^{-1}.

	Neat IL	16.6 mol %/IL	35 mol %/IL: DGME	35 mol %/DGME	16.6 mol %/IL:DGME	16.6 mol %/DGME
i_{cis}/i_{trans}	0.78	0.87	0.79	0.74	0.66	0.58

Table 3. ^{23}Na chemical shift, peak width, and physicochemical properties of samples at 20 °C.

Sample	δ [ppm]	Peak width [Hz]	Conductivity [mS cm^{-1}]	Viscosity [mPa s]
16.6 mol %/IL	−11.2	637.0	0.8	344.2
35 mol %/IL:DGME	−6.7	660.0	1.2	112.2
35 mol %/DGME	−6.0	435.0	2.3	53.2
16.6 mol %/IL:DGME	−5.4	217.0	6.6	15.2
16.6 mol %/DGME	−5.4	128.0	9.3	4.9

active bands relating to the vibration of SO_2 and CF_3 bonds, (Figure 5a). The possible conformers for the TFSI anion are either *cis*, where the CF_3 groups are in the same plane, or *trans*, where they are in a different plane, relative to the S–N–S plane of TFSI. In either case, the TFSI would mainly predominantly coordinate to Na^+ through the oxygen atoms of the SO_2 group. According to the literature, the bands appearing at 1348 and 1330 cm^{-1} (Figure 5a) correspond to the SO_2 antisymmetric stretching in-phase and out-of-phase with a higher contribution of *trans* and *cis* conformers, respectively.[17] The band at 1133 cm^{-1} corresponds to the SO_2 symmetric stretching in-phase.[17]

As shown in Figure 5a, in comparison with the neat IL, there is a slight shift towards higher wavenumbers in both electrolyte compositions (35 and 16.6 mol% IL:DGME), which is related to the interaction between $TFSI^-$ and Na^+. However, no shift in wavenumber could be found between the 35 and 16.6 mol%/IL:DGME electrolytes, exemplifying little differences on the Na^+ speciation at these concentrations (Figure 5a). A closer examination of the bands reflects a trend in the conformer contribution when comparing the relative intensities of the SO_2 antisymmetric stretching (i_{cis}/i_{trans}) are considered for *cis* at 1352 cm^{-1} and *trans* at 1333 cm^{-1} (Figure 5b, Table 2).

As reported in the literature, in neat TFSI-based ILs, the *trans* conformer tends to be more thermodynamically stable than *cis*; although both species are present in equilibrium.[17d,18] A progressive increase in the proportion of the *cis* TFSI conformer upon salt addition in neat ionic liquids has previously been reported for other TFSI-based ionic liquids.[19] In this study, an increase of the *cis* conformer contribution from the neat IL was observed (i_{cis}/i_{trans}: 0.78 to 0.87 in the 16.6 mol%/IL (without DGME, Table 2)). However, by increasing the amount of DGME in the electrolyte, the *trans* conformer is favoured due to the displacement of TFSI by DGME. This can be explained by a complete coordination of Na^+ by DGME leading to a higher amount of free TFSI in the bulk. In the case of the 35 mol% salt concentration, the conformer ratio remains similar and mostly in the *cis* conformation regardless of the solvent composition; since there is a deficiency of DGME, this allows coordination of the Na^+ cations to TFSI anion.

2.2. NMR Spectroscopy

In order to study the solvation and dynamics of Na^+ in the studied mixtures ^{23}Na nuclear magnetic resonance (NMR) experiments were performed. As depicted in Figure 6a, the ^{23}Na chemical shift is affected by the concentrations in the electrolyte mixtures. The chemical shift of Na^+ in the presence of neat ionic liquid (16.6 mol%/IL) is −11.2 ppm, which is consistent with our previous studies in a similar electrolyte, NaFSI in *N*-methyl-*N*-propyl pyrrolidinium bis(fluorosulfonyl)imide, [C_3mpyr][FSI].[20] However, upon modifying the composition of the electrolyte from 16.6 mol%/DGME to 16.6 mol%/IL:DGME, the ^{23}Na resonance occurs at the more positive value of −5.4 ppm (Table 3) in both electrolyte mixtures.

The NMR observations can been explained in terms of the Gutmann donor number (DN) correlation with ligand solvation strength, which is directly proportional to the ^{23}Na chemical shift.[21] On that basis, a more positive ^{23}Na chemical shift is expected with strongly coordinating ligands (high DN)[4b,21–22] such as DGME (DN: 19.5 kcal mol^{-1}), whereas a more negative value is expected when only TFSI coordination is significant due to its low DN (5.4 kcal mol^{-1}).[22c,23] Thus, for the 35 mol%/IL:DGME the resonance is detected at more negative values (−6.7 ppm) because of the mixed coordination mode of Na^+ to both DGME and TFSI, than in 16.6 mol%/IL:DGME (−5.4 ppm)

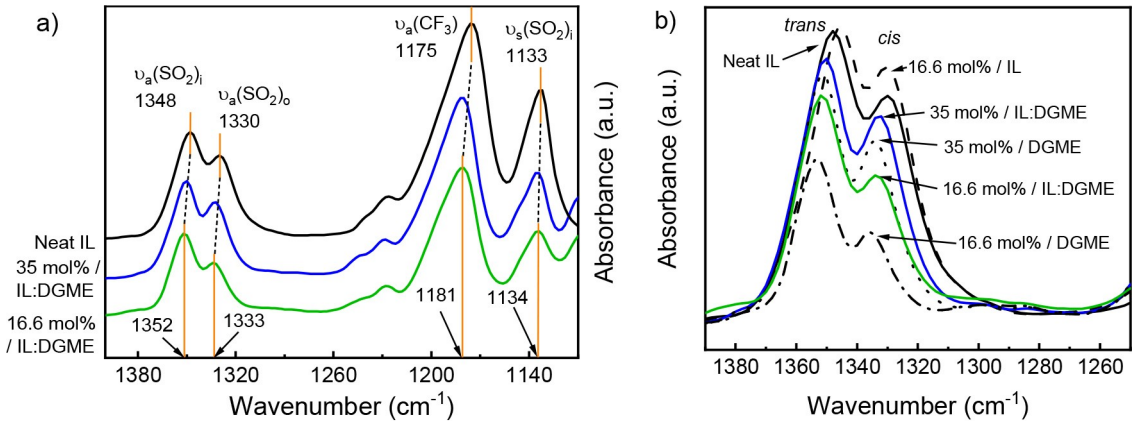

Figure 5. FTIR spectra for the TFSI regions of a) 1390–1130 cm^{-1} and b) 1390–1250 cm^{-1}.

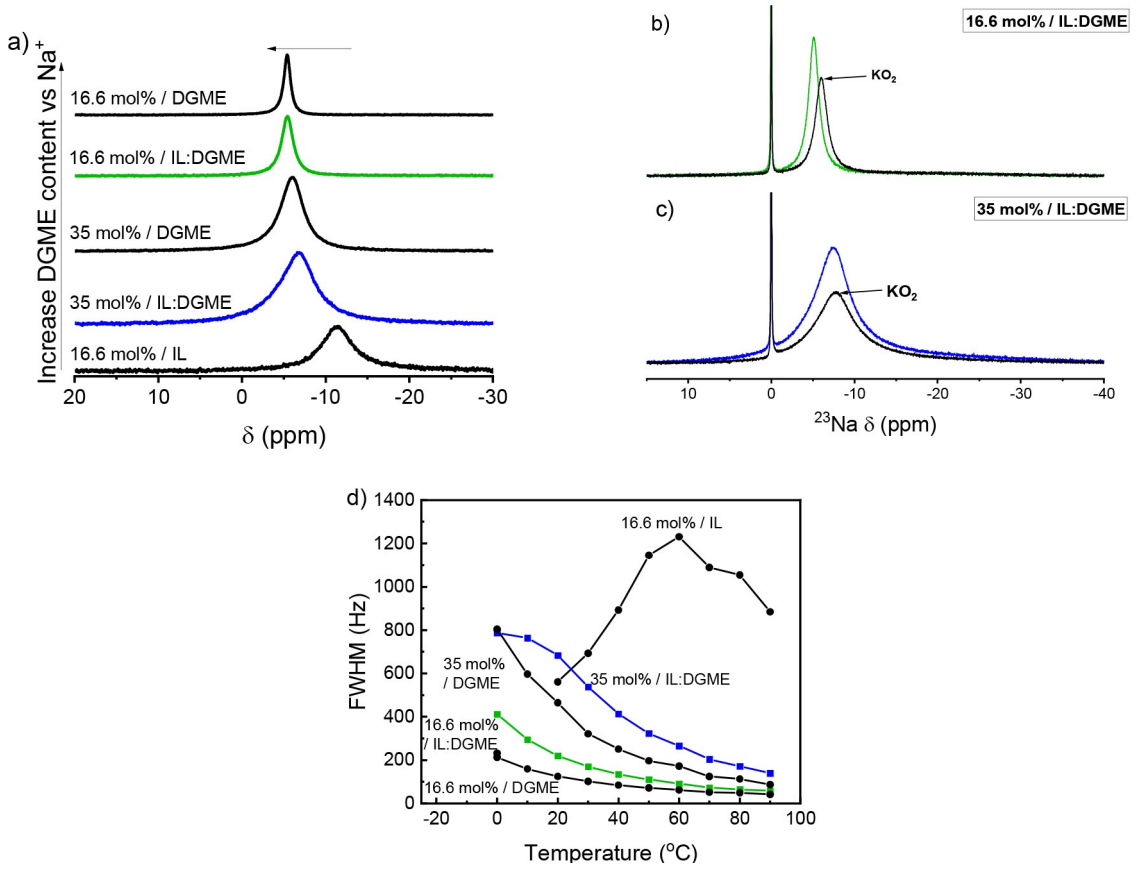

Figure 6. a) ^{23}Na NMR chemical shift, comparison of the ^{23}Na chemical shifts relative to NaF in the presence (black) and absence of KO_2 for b) 16.6 mol%/IL:DGME (green) and c) 35 mol%/IL:DGME (blue). NaF signal around 0 ppm used as reference and (d) peak width of the different electrolytes studied. Adapted figure from Ref. [13] with permission. Copyright (2020), American Chemical Society.

where Na^+ is almost exclusively coordinated to DGME, as a consequence of the high free DGME content as quantified in. Clearly, the presence of DGME (in excess or deficit) has a strong influence on the ^{23}Na chemical shift.

The stronger interaction between sodium cations and the electrolyte would explain the larger size of the discharge products (average size ~3.5 μm) (Figure 1) generated in the 16.6 mol%/IL:DGME electrolyte as this is related to the larger desolvation energy required for deposition, which facilitates a lower discharge deposition mechanism. Moreover, the fact that the 16.6 mol%/DGME and IL:DGME samples gives the same sodium chemical shift (−5.4 ppm) in the absence or presence of IL, shows the low participation of IL in the sodium solvation which is dominated by DGME.

To provide a more relevant scenario to the battery performance during cycling, KO_2 was added to the electrolytes as a

source of superoxide anion, which is the oxygen electrogenerated species formed during the discharge process. In these samples, the three species competing for the solvation of Na^+ are DGME, TFSI and $O_2^{\bullet-}$.

In general, the ^{23}Na chemical shift becomes more negative in the presence of $O_2^{\bullet-}$, suggesting a change in the sodium solvation shell (Figure 6b and c). This could arise from the interaction of Na^+ with superoxide, which displaces the original ligands (DGME and TFSI). However, the extent of the effect depends on the composition of the electrolyte. For example, a more negative chemical shift is obtained in the 16.6 mol%/IL:DGME electrolyte in the presence of KO_2 (from −5.1 ppm without KO_2 to −6.1 ppm with KO_2) than with the 35 mol%/IL:DGME electrolyte (from −7.4 ppm without KO_2 to −7.8 ppm with KO_2). This suggests a greater influence of $O_2^{\bullet-}$ on the coordination environment of Na^+ in 16.6 mol% due to weakening of the interaction of Na^+ with DGME, whereas in the more concentrated electrolyte this effect is less pronounced because of the lower DGME content. However, it is important to consider the paramagnetic effect of superoxide anion and the influence, to some degree, in the chemical shift.

In general, the ^{23}Na peak width depends on both the symmetry of the local coordination environment around the Na^+ and the dynamics (e.g. rotational motions or exchange) in the media. In turn the peak width may be related to the deposition mechanism of the discharge product. At 20 °C, the peak width decreases with increasing concentration of DGME, from 660.0 Hz for the 35 mol%/IL:DGME electrolyte to 128.0 Hz for the 16.6 mol%/DGME electrolyte (Table 3). This peak sharpening is consistent with increased local dynamics associated with decreased viscosity of the electrolyte in the samples with higher DGME content (e.g. 4.9 mPa s and 9.3 mS cm^{-1} for the 16.6 mol%/DGME) (Table 3).

Interestingly, although the chemical shift is the same for the samples with DGME in excess (16.6 mol%/DGME and IL:DGME), the peak width is increased in the presence of IL. As evident in Table 3, the 16.6 mol%/IL:DGME electrolyte has lower conductivity and higher viscosity than the sample without IL (6.6 vs 9.3 mS cm^{-1} and 15.2 vs 4.9 mPa s, respectively). The sodium diffusion coefficient (D_{Na^+}) was determined by pulsed-field gradient ^{23}Na NMR for these two samples, from 30 to 90 °C. A higher D_{Na^+} value was obtained for 16.6 mol%/DGME (i.e. 1.24×10^{-10} m^{2}s^{-1} vs 1.94×10^{-10} m^{2}s^{-1} at 80 °C), which follows the trend of the viscosity and conductivity (Table 3). In addition, the much slower sodium dynamics found in the 35 mol%/IL:DGME, could due to the higher viscosity of this electrolyte compared to its homologous 16.6 mol%/IL:DGME (112.2 vs 15.2 mPa s, respectively).

However, it is not possible to conclude that variation in the sodium dynamics is solely responsible for the differences in the battery performance. As reported above, factors such as the Na^+ solvation shell composition, the identity of TFSI conformers and the amount of free and coordinated DGME also play an important role in the performance. The presence of free DGME seems to be an important factor in the different morphology of the discharge products and in turn in the battery performance. A control study using an electrolyte with just two molecules of DGME per Na^+ was also characterised, showing a discharge capacity similar to the 35 mol%/IL:DGME (ca. 2.8 mAh cm^{-2}). In that case, the discharge product covers a large area of the air cathode, with larger particle size (average size ≈4.7 μm) than using the 16 mol%/IL:DGME electrolyte (Figure SI 2). Most likely, for the later, the discharge products are soluble in the excess of DGME following a solution mediated mechanism, as opposed to the other electrolyte compositions.

On the basis of conductivity and viscosity, the largest peak width in Figure 6d would be expected for the 16.6 mol%/IL (in the absence of DGME); however, the peak width was narrower than the 35 mol%/IL:DGME (637.0 vs 660.0 Hz respectively). A possible explanation could be a more symmetric solvation shell which will result in a smaller quadrupolar interaction and hence a narrower peak width. However, as reported in the literature for Na^+ in IL-based electrolytes, the peak width profile presents two relaxation mechanisms: region i) rapid site exchange broadening mechanism, usually present at lower temperatures, and region ii) motion induced line narrowing, at higher temperatures.[11f] In the present case, peak width studies over temperature from 0 to 90 °C displayed motion induced narrowing (region ii) for the entire temperature range for all compositions. However, 16.6 mol%/IL exhibits both regions (Figure 6b) and at 20 °C, is the only sample displaying a rapid exchange mechanism, showing a narrower peak than expected.

2.3. Modelling in the Absence of Superoxide Anion

Computational experiments provide further understanding of the solvation structure of Na^+ and the superoxide anion in 35 mol% and 16.6 mol%/IL:DGME. The types of coordination were predicted by calculating the radial distribution function (RDF), which shows the probability of finding an atom/molecule at a certain distance from another atom centre when one of them is at the origin. The Na^+ coordination numbers (CN) also were calculated as in our previous work.[13] In summary, since the 16.6 mol%/IL:DGME system has excess DGME, most Na^+ ions are solvated by two DGME molecules – $[Na(DGME)_2]^+$ –, although there is a small amount of TFSI also participating in the Na^+ nearest to the coordination shell, as shown in Figure 7a. In the 35 mol%/IL:DGME system, since the number of TFSI molecules relative to DGME increases, the Na^+ coordination environment becomes diversified, including $[Na(DGME)_2]^+$, $[Na(DGME)_2(TFSI)_x]^{1-x}$, $[Na(DGME)(TFSI)_x]^{1-x}$, and $[Na(TFSI)_x]^{1-x}$. This is indicated by colour coding of the Na ions in Figure 7d–f, where Na ions in $[Na(TFSI)_3]^{2-}$ are coloured in green, those in $[Na(DGME)_2]^+$ are in blue, and those in hybrid coordination structures are in purple.

This is in contrast to the 16.6 mol%/IL:DGME system, in which Na^+ only has two types of coordination. Another substantial change is the number of free DGME molecules (black stick) that do not coordinate to Na^+ as indicated in Figure 7b and e, very obvious in the less concentrated system which is consistent with the result from FTIR analysis.

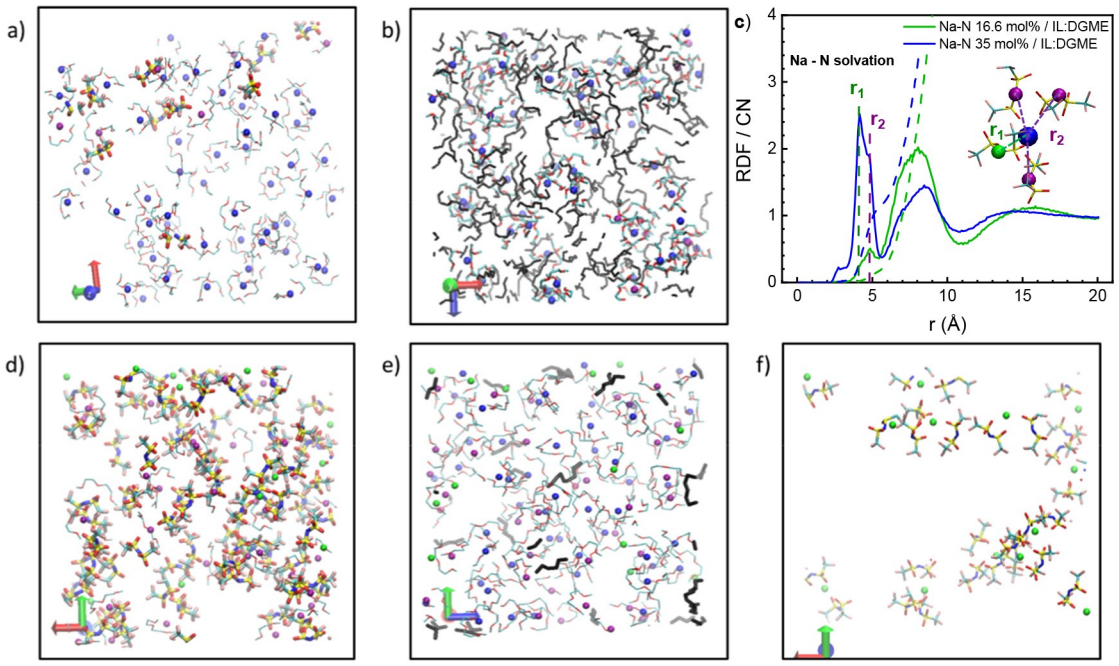

Figure 7. Snapshots of selected DGME, Na^+ and TFSI data that provide structural information in the a–b) 16.6 mol%/IL:DGME and d-f) 35 mol%/IL:DGME systems. (a) highlights two types of Na^+ coordination environments with DGME only (blue Na^+) or with both DGME and TFSI (purple Na^+). (b) highlights two types of DGME that coordinate to (green sticks) or do not coordinate to (black sticks) Na^+. (d) shows the increase in Na^+-TFSI coordination where green and purple Na^+ ions are coordinated to TFSI only or with both TFSI (bold sticks) and DGME (thin sticks), respectively. (e) highlights three types of Na^+ and two types of DGME using same colour coding as above. (f) highlights the Na^+ coordination to TFSI only in the 35 mol% system. (c) compares RDFs of Na^+-N(TFSI) for the 16.6 mol% and 35 mol% systems with the inset highlighting bidentate (r_1) and monodentate (r_2) coordination between Na^+ and TFSI, corresponding to overlapping RDF peaks between 3.5 and 6 Å.

Bidentate (Na coordinates to O atoms from both SO_2 groups) and monodentate (Na coordinates to O atoms from one SO_2 group) coordination are usually found represented by the split peak within 6 Å in Na–N RDF (Figure 7c). The monodentate coordination is more common in the high salt concentration IL systems due to the formation of Na-anion aggregates, whereas the bidentate coordination is dominant in the low salt concentration system. One example is seen in the pyrrolidinium-based IL with the bis(fluorosulphonyl)imide anion.[24] Interestingly, Figure 7c shows a different change in Na-TFSI coordination geometry than reported in the literature. For instance, there is a higher percentage of bidentate Na-TFSI coordination structures in the 35 mol%/IL:DGME system, which actually has a higher Na salt concentration than the 16.6 mol%/IL:DGME system. This is indicated by the higher intensity at r_1 (bidentate) than at r_2 (monodentate) in the 35 mol% system. The inset diagram included in Figure 7c highlights the different coordination geometries of the TFSI. For Na^+ sharing their coordination with TFSI and DGME, the bidentate Na-TFSI coordination is more favourable; whereas in the 16.6 mol% system in which Na^+ is in a $[Na(DGME)_2(TFSI)]$ complex, the monodentate is more likely to form due to steric hindrance by two DGME molecules.

Since bidentate coordination is more stable than the monodentate coordination, the deposition mechanism should be slower for the 35 mol%-based electrolyte, thus resulting in larger discharge products. However, the opposite outcome is observed in these electrolytes (average size ~2.5 μm, figure 1) and this can be explained by the diglyme governing the deposition mechanism due to a stronger interaction with Na^+. Thus, considering the full coordination of Na^+ by diglyme in the 16.6 mol% solution, larger discharge products (average size ~3.5 μm) were formed.

2.4. Modelling in the Presence of Superoxide Anion

The impact of superoxide anions on the solvation shell of Na^+ was also studied by incorporating a small number of superoxide species in both systems to mimic the low solubility of superoxide in the electrolytes. Certainly, all $O_2^{\bullet-}$ immediately interact in the nearest coordination shell of Na^+ as seen in the snapshots in Figure 8g and h. However, due to the low amount of $O_2^{\bullet-}$, they have a very low effect on Na-DGME and Na-TFSI coordination. $O_2^{\bullet-}$ hardly affects the Na-DGME coordination number, as shown in Figure 8a and d, and only slightly changes the Na-TFSI coordination number at the first RDF peak around 6 Å. The CN of Na-TFSI increases slightly in the 16.6 mol% system (Figure 8b), but decreases slightly instead for the 35 mol% system (Figure 8e), suggesting that $O_2^{\bullet-}$ can participate in the Na coordination shell with both DGME and TFSI. The $O_2^{\bullet-}$ can facilitate the Na-TFSI coordination when it is less in the 16.6% system but could disturb its coordination when it becomes more common in the 35% system. We also observe that the presence of $O_2^{\bullet-}$ also leads to Na ion aggregation in both electrolyte solutions, as indicated by the prominent peaks

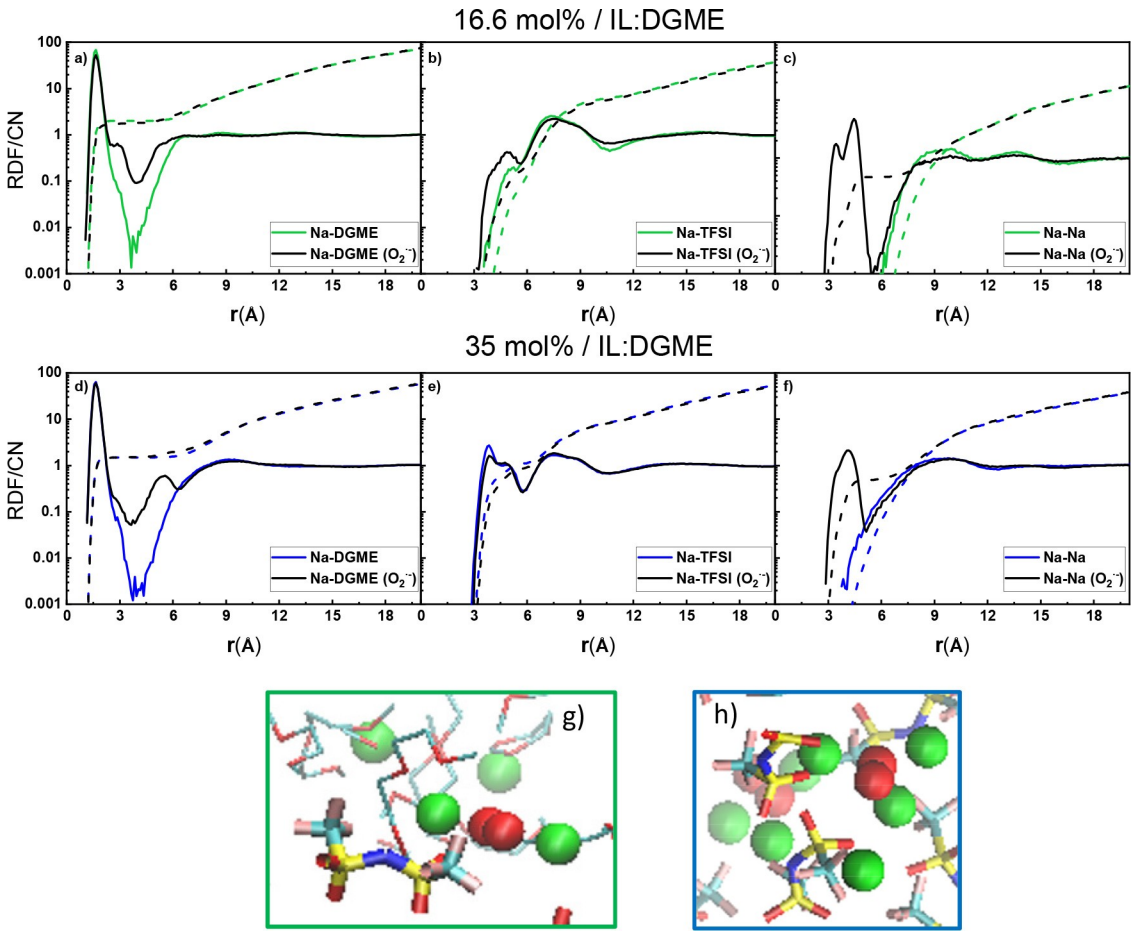

Figure 8. RDF and CN data for the 16.6 (top row) and 35 mol% (bottom row)/IL:DGME showing the Na–Na interactions in a) and d) Na-DGME, b) and e) Na-TFSI and c) and f) in the absence (coloured line) and presence (black line) of $O_2^{\bullet-}$. g) and h) show the snapshots for the 16.6 and 35 mol% respectively in presence of superoxide. Colour code: O (red), N (blue), C (cyan), F (pink), S (yellow) and Na (green).

between 3 and 6 Å for Na–Na RDF in the system with the presence of $O_2^{\bullet-}$ (Figure 8c and f). The same Na^+-$O_2^{\bullet-}$ coordination environment has previously been reported by Tatara et al. for a NaTFSI:DME system, where the coordination of the superoxide was two $[Na(DME)_2]^+$, more energetically favoured than just one $[Na(DME)_2]^+$.[5]

3. Conclusions

In this work, the speciation in the bulk electrolyte for two $[C_4mpyr][TFSI]$:DGME hybrid electrolyte systems (16.6 and 35 mol% NaTFSI) has been investigated and the relevance to the electrochemical behaviour of these hybrid electrolytes established. A stronger interaction between Na^+ and DGME in the 16.6 mol%/IL:DGME electrolyte was identified, which explains the larger sized discharge products, larger desolvation energy and difference in deposition mechanisms, most likely solution mediated growth, as a result of the free DGME in the system. In addition, the low participation of the IL in Na^+ solvation was confirmed by NMR spectroscopy, showing that solvation is highly dominated by DGME.

In the presence of KO_2, the Na^+-$O_2^{\bullet-}$ interaction is more favourable than that with DGME, so DGME is replaced by superoxide. This facilitates a greater impact of $O_2^{\bullet-}$ in the coordination environment of Na^+ in the case of the 16.6 mol% system, than in the 35 mol% electrolyte with a lower DGME content. Additionally, higher Na^+ mobility was observed for the 16.6 mol%/IL:DGME by NMR, which provides superior physicochemical properties for this system. Bidentate coordination and a larger population of *cis* TFSI conformers was found for the 35 mol%-based electrolyte, which could imply more nucleation sites and smaller discharge products. The opposite trend is observed in the 16.6 mol%-based electrolyte, where diglyme governs the deposition mechanism. Thus, the full and stronger coordination of Na^+ by DGME in the 16.6 mol% solution leads to fewer nucleation sites and formation of larger discharge products.

This study establishes the critical parameters that affect Na–O_2 battery performance in these recently discovered hybrid electrolytes. Understanding the ion-electrolyte interactions, Na^+ solvation, coordination and physicochemical properties can provide a key to advancing this area of battery technology by facilitation of the development of stable electrolytes on a rational basis.

Acknowledgements

L.G.-Q., F.C., P.C.H., M.F., and C.P.-G. gratefully acknowledge financial support from the Australian Research Council (ARC) through the ARC Centre of Excellence for Electromaterials Science (ACES) (Project ID: CE140100012). F.C. acknowledges computing resources provided at the NCI National Facility systems at the Australian National University through the National Computational Merit Allocation Scheme supported by the Australian Government. Deakin University's Advanced Characterisation Facility is acknowledged for use of the NMR instrumentation. N.O.-V. also acknowledges the Basque Government (Elkartek CICe2020, KK-2020/00078) for the financial support of this work.

Conflict of Interest

The authors declare no conflict of interest.

Keywords: Glymes · ionic liquids · oxygen · sodium-oxygen · solvation · superoxide

[1] a) P. Hartmann, C. L. Bender, M. Vračar, A. K. Dürr, A. Garsuch, J. Janek, P. Adelhelm, *Nat. Mater.* **2012**, *12*, 228; b) W. W. Yin, Z. W. Fu, *ChemCatChem* **2017**, *9*, 1545–1553; c) S. Ha, J. K. Kim, A. Choi, Y. Kim, K. T. Lee, *ChemPhysChem* **2014**, *15*, 1971–1982.

[2] a) S. Kang, Y. Mo, S. P. Ong, G. Ceder, *Nano Lett.* **2014**, *14*, 1016–1020; b) Y. S. Mekonnen, R. Christensen, J. M. Garcia-Lastra, T. Vegge, *J. Phys. Chem. Lett.* **2018**, *9*, 4413–4419.

[3] N. Ortiz Vitoriano, I. Ruiz de Larramendi, R. L. Sacci, I. Lozano, C. A. Bridges, O. Arcelus, M. Enterría, J. Carrasco, T. Rojo, G. M. Veith, *Energy Storage Mater.* **2020**, *29*, 235–245.

[4] a) L. Lutz, W. Yin, A. Grimaud, D. Alves Dalla Corte, M. Tang, L. Johnson, E. Azaceta, V. Sarou-Kanian, A. Naylor, S. Hamad, *J. Phys. Chem. C* **2016**, *120*, 20068–20076; b) P. Geysens, V. S. Rangasamy, S. Thayumanasundaram, K. Robeyns, L. Van Meervelt, J.-P. Locquet, J. Fransaer, K. Binnemans, *J. Phys. Chem. B* **2018**, *122*, 275–289.

[5] R. Tatara, G. M. Leverick, S. Feng, S. Wan, S. Terada, K. Dokko, M. Watanabe, Y. Shao-Horn, *J. Phys. Chem. C* **2018**, *122*, 18316–18328.

[6] a) R. Black, A. Shyamsunder, P. Adeli, D. Kundu, G. K. Murphy, L. F. Nazar, *ChemSusChem* **2016**, *9*, 1795–1803; b) K. U. Schwenke, S. Meini, X. Wu, H. A. Gasteiger, M. Piana, *Phys. Chem. Chem. Phys.* **2013**, *15*, 11830–11839; c) S. A. Freunberger, Y. Chen, N. E. Drewett, L. J. Hardwick, F. Bardé, P. G. Bruce, *Angew. Chem. Int. Ed.* **2011**, *50*, 8609–8613; *Angew. Chem.* **2011**, *123*, 8768–8772.

[7] I. Lozano, I. R. de Larramendi, N. Ortiz-Vitoriano, *Materials Research Foundations, Vol. 76*, Materials Research Forum LLC, **2020**, pp. 205–228.

[8] a) Q. Yang, Z. Zhang, X.-G. Sun, Y.-S. Hu, H. Xing, S. Dai, *Chem. Soc. Rev.* **2018**, *47*, 2020–2064; b) M. Kar, T. J. Simons, M. Forsyth, D. R. MacFarlane, *Phys. Chem. Chem. Phys.* **2014**, *16*, 18658–18674; c) M. Armand, F. Endres, D. R. MacFarlane, H. Ohno, B. Scrosati, *Nat. Mater.* **2009**, *8*, 621; d) S. A. Forsyth, J. M. Pringle, D. R. MacFarlane, *Aust. J. Chem.* **2004**, *57*, 113–119; e) A. Basile, M. Hilder, F. Makhlooghiazad, C. Pozo-Gonzalo, D. R. MacFarlane, P. C. Howlett, M. Forsyth, *Adv. Energy Mater.* **2018**, *8*, 1703491.

[9] a) Y. Katayama, K. Sekiguchi, M. Yamagata, T. Miura, *J. Electrochem. Soc.* **2005**, *152*, E247-E250; b) L. Grande, E. Paillard, G.-T. Kim, S. Monaco, S. Passerini, *Int. J. Mol. Sci.* **2014**, *15*, 8122–8137; c) S. Monaco, A. M. Arangio, F. Soavi, M. Mastragostino, E. Paillard, S. Passerini, *Electrochim. Acta* **2012**, *83*, 94–104; d) C. Pozo-Gonzalo, L. R. Johnson, E. Jónsson, C. Holc, R. Kerr, D. R. MacFarlane, P. G. Bruce, P. C. Howlett, M. Forsyth, *J. Phys. Chem. C* **2017**, *121*, 23307–23316; e) C. Pozo-Gonzalo, P. C. Howlett, D. R. MacFarlane, M. Forsyth, *Electrochem. Commun.* **2017**, *74*, 14–18; f) S. Das, J. Højberg, K. B. Knudsen, R. Younesi, P. Johansson, P. Norby, T. Vegge, *J. Phys. Chem. C* **2015**, *119*, 18084–18090; g) G. A. Elia, J. Hassoun, W. J. Kwak, Y. K. Sun, B. Scrosati, F. Mueller, D. Bresser, S. Passerini, P. Oberhumer, N. Tsiouvaras, J. Reiter, *Nano Lett.* **2014**, *14*, 6572–6577.

[10] Y. Zhang, N. Ortiz-Vitoriano, B. A. Acebedo, L. O'Dell, D. R. MacFarlane, T. F. Rojo, M. Forsyth, P. C. Howlett, C. Pozo-Gonzalo, *J. Phys. Chem. C* **2018**, *122*, 15276–15286.

[11] a) F. Makhlooghiazad, P. C. Howlett, X. Wang, M. Hilder, D. R. MacFarlane, M. Armand, M. Forsyth, *J. Mater. Chem. A* **2017**, *5*, 5770–5780; b) K. Periyapperuma, E. Arca, S. Harvey, C. Ban, A. Burrell, D. R. MacFarlane, C. Pozo-Gonzalo, M. Forsyth, P. C. Howlett, *J. Mater. Chem. A* **2020**, *8*, 3574–3579; c) K. Matsumoto, Y. Okamoto, T. Nohira, R. Hagiwara, *J. Phys. Chem. C* **2015**, *119*, 7648–7655; d) Y. Yamada, M. Yaegashi, T. Abe, A. Yamada, *Chem. Commun.* **2013**, *49*, 11194–11196; e) H. Yoon, P. Howlett, A. S. Best, M. Forsyth, D. R. Macfarlane, *J. Electrochem. Soc.* **2013**, *160*, A1629; f) H. Yoon, H. Zhu, A. Hervault, M. Armand, D. R. MacFarlane, M. Forsyth, *Phys. Chem. Chem. Phys.* **2014**, *16*, 12350–12355.

[12] a) N. Plylahan, M. Kerner, D.-H. Lim, A. Matic, P. Johansson, *Electrochim. Acta* **2016**, *216*, 24–34; b) F. Makhlooghiazad, C. Pozo-Gonzalo, P. Johansson, M. Forsyth, in *Na-ion Batteries* (Eds.: L. Monconduit, L. Croguennec), ISTE Ltd and Wiley, London and New York, **2020**; c) M. Montanino, M. Moreno, M. Carewska, G. Maresca, E. Simonetti, R. L. Presti, F. Alessandrini, G. Appetecchi, *J. Power Sources* **2014**, *269*, 608–615; d) B. Yang, C. Li, J. Zhou, J. Liu, Q. Zhang, *Electrochim. Acta* **2014**, *148*, 39–45.

[13] N. Ortiz-Vitoriano, I. Monterrubio, L. Garcia-Quintana, J. M. López del Amo, F. Chen, T. Rojo, P. C. Howlett, M. Forsyth, C. Pozo-Gonzalo, *ACS Energy Lett.* **2020**, *5*, 903–909.

[14] a) V. Seneviratne, R. Frech, J. E. Furneaux, M. Khan, *J. Phys. Chem. B* **2004**, *108*, 8124–8128; b) P. Johansson, J. Grondin, J.-C. Lassègues, *J. Phys. Chem. A* **2010**, *114*, 10700–10705.

[15] R. Frech, W. Huang, *Macromolecules* **1995**, *28*, 1246–1251.

[16] P. Johansson, J. Grondin, J.-C. Lassègues, *J. Phys. Chem. A* **2010**, *114*, 10700–10705.

[17] a) P. Howlett, N. Brack, A. Hollenkamp, M. Forsyth, D. MacFarlane, *J. Electrochem. Soc.* **2006**, *153*, A595-A606; b) J. Kiefer, J. Fries, A. Leipertz, *Appl. Spectrosc.* **2007**, *61*, 1306–1311; c) L. J. Hardwick, J. A. Saint, I. T. Lucas, M. M. Doeff, R. Kostecki, *J. Electrochem. Soc.* **2009**, *156*, A120-A127; d) J.-C. Lassègues, J. Grondin, C. Aupetit, P. Johansson, *J. Phys. Chem. A* **2009**, *113*, 305–314; e) V. H. Paschoal, L. F. Faria, M. C. Ribeiro, *Chem. Rev.* **2017**, *117*, 7053–7112.

[18] a) M. Herstedt, M. Smirnov, P. Johansson, M. Chami, J. Grondin, L. Servant, J. Lassegues, *Journal of Raman Spectroscopy: An International Journal for Original Work in all Aspects of Raman Spectroscopy, Including Higher Order Processes, and also Brillouin and Rayleigh Scattering* **2005**, *36*, 762–770; b) J. C. Lassègues, J. Grondin, R. Holomb, P. Johansson, *J. Raman Spectrosc.* **2007**, *38*, 551–558.

[19] a) H. Kondo, M. Matsumiya, K. Tsunashima, S. Kodama, *Electrochim. Acta* **2012**, *66*, 313–319; b) O. Palumbo, F. Trequattrini, F. M. Vitucci, M. A. Navarra, S. Panero, A. Paolone, *Advances in Condensed Matter Physics* **2015**, *2015*, 176067; c) Y. Umebayashi, T. Mitsugi, S. Fukuda, T. Fujimori, K. Fujii, R. Kanzaki, M. Takeuchi, S.-I. Ishiguro, *J. Phys. Chem. B* **2007**, *111*, 13028–13032; d) J.-C. Lassègues, J. Grondin, D. Talaga, *Phys. Chem. Chem. Phys.* **2006**, *8*, 5629–5632; e) M. Matsumiya, T. Yamada, S. Murakami, Y. Kohno, K. Tsunashima, *Solvent Extr. Ion Exch.* **2016**, *34*, 454–468.

[20] M. Forsyth, H. Yoon, F. Chen, H. Zhu, D. R. MacFarlane, M. Armand, P. C. Howlett, *J. Phys. Chem. C* **2016**, *120*, 4276–4286.

[21] R. H. Erlich, A. I. Popov, *J. Am. Chem. Soc.* **1971**, *93*, 5620–5623.

[22] a) W. Linert, A. Camard, M. Armand, C. Michot, *Coord. Chem. Rev.* **2002**, *226*, 137–141; b) K. Abraham, *J. Electrochem. Soc.* **2015**, *162*, A3021-A3031; c) I. Geoffroy, P. Willmann, K. Mesfar, B. Carré, D. Lemordant, *Electrochim. Acta* **2000**, *45*, 2019–2027.

[23] M. Barghamadi, A. S. Best, A. I. Bhatt, A. F. Hollenkamp, P. J. Mahon, M. Musameh, T. Rüther, *Electrochim. Acta* **2015**, *180*, 636–644.

[24] F. Chen, P. C. Howlett, M. Forsyth, *J. Phys. Chem. C* **2017**.

Manuscript received: November 6, 2020
Accepted manuscript online: November 23, 2020
Version of record online: December 10, 2020